Decoding Alumina Dissolution by Navigating the Dynamic Interplay of Bath Composition

Jonathan Alarie[1], Martin Truchon[2], László Kiss[3], Lukas Dion[3], Sébastien Guérard[4] and Jean-François Bilodeau[5]
1. PhD Student
2. Technician
3. Professor
Université du Québec à Chicoutimi (UQAC), GRIPS, REGAL, CURAL, Saguenay, Canada
4, 5. Research scientist
Rio Tinto Arvida Research and Development Centre, Saguenay, Canada
Corresponding author: jonathan.alarie1@uqac.ca
https://doi.org/10.71659/icsoba2024-al018

Abstract

Efficient dissolution of alumina is essential to maintain ideal conditions in an aluminium reduction cell. Too little alumina dissolved in the electrolyte provokes the so-called anode effect, while a surplus favours the muck formation under the metal pad. In the two cases, the energetic and environmental performance of the electrolysis cell decreases rapidly, in opposition to the priorities of the aluminium industry.

This work presents an intricate model to reproduce the alumina dissolution process to assess the influence of the chemistry and bath properties on the alumina dissolution kinetics.

Simulation results are compared with the ones obtained from an extensive experimental parametric study to validate the behaviour and understand the kinetics involved. From these results, the limiting factor to the raft dissolution is the internal diffusivity of the dissolved alumina. An increase of the fluoride content, aluminium, and calcium, within the bath increases the diffusivity of the dissolved alumina, thus increasing its dissolution rate. However, this beneficial impact can be counterbalanced by the lower solubility of the alumina in the bath. Accordingly, the relationship between the bath composition and the raft dissolution kinetics is presented at different superheats to understand this delicate equilibrium. Subsequently, the differences in the dissolution conditions between the experimental setup and industrial cells are described. Finally, a pathway to reach an optimal composition for industrial cells is presented.

Keywords: Alumina rafts, Bath composition, Alumina dissolution.

1. Introduction

The production of primary aluminium through the Hall-Héroult process needs a constant input of alumina to sustain the reaction. Therefore, alumina powder is fed every minute or so at three to five points in the electrolysis cell. These injections of typically one kilogram of alumina rapidly aggregate to form solid rafts that are difficult to dissolve and create a significative lag between the injection and the reduction. Moreover, undissolved alumina can migrate in the electrolysis cell creating spatial heterogeneity in the dissolved alumina concentration. The spatial and temporal heterogeneity create instabilities in the electrolysis process, such as anode effect or muck formation, which promotes instability, loss of production, greenhouse gas generation, and degradation of the cell. With such a focus on energy efficiency and environmental emissions reduction, a deep understanding of alumina dissolution is essential to maintain the process in a narrower band of stability. In this way, the work presented here compares experimental results obtained with a gravimetric method to a unidimensional model, previously presented in [1],

relying solely on the bath chemistry and the temperature of the bath and alumina to predict the dissolution behaviour of powdered alumina.

2. Methodology

2.1 Experiments

This study is based on two elements, aiming to compare the results from several laboratory experiments to a one-dimensional alumina dissolution model to assess the latter's accuracy. The gravimetric method was employed to create alumina powder injection samples in cryolite baths of various chemical and thermal conditions. A stainless-steel ring with a diameter of 12 cm was brought down to the bath-air interface level. The ring also had overlapping wires at the interface level. Then a mass of 40 grams of alumina was injected using a funnel to the bath surface and constrained to the ring dimensions. This enabled the alumina to attach to the metal ring and the horizontal pins at its bottom wires. Subsequently, the apparent weight of our samples was monitored as they underwent infiltration, sintering, and dissolution.

In the meantime, a video recording of the sample was made. This was helpful to the understanding of the behaviour observed in the gravimetric curves. However, the top of the furnace needed to be open for visual access during the whole test. This created a large radiative heat loss on the top of the bath and the sample. Therefore, the initial superheat of the cryolitic bath was increased by 5 °C before the injection. In most cases, the heat losses decreased the bath temperature steadily by an amount of about 20°C from the beginning to the end of the test. This value depends on the condition used but was uniformly imposed on the model calculations.

Three injections using primary alumina were done for each of the five test conditions. Since the same electrolytic bath is used, a slight change in the alumina mass fraction of the electrolyte is present between each sample. Worst-case scenario calculations indicate that the augmentation of concentration is lower than 0.3 % between each reported test. However, as the complete dissolution of the samples was only achieved in a few cases, the plausible change in concentration is even lower than 0.3 %.

2.2 Mathematical Modelling

For the scope of this study, a model presented at TMS 2024 was reused [1]. An important hypothesis of this model is that the alumina injection dynamic is so fast that no crust can be created around the heap of powder. The bath solidification is only considered when the particles are at rest. This hypothesis was allowed by the observation of the video recording of the experimental tests. During these tests, the infiltration front of the sample moves almost constantly toward the centre of the raft. This invalidates the hypothesis that a solid crust shell is present around the alumina because that phenomenon would prevent the continuous infiltration of the raft. In the meantime, Figure 1 shows the progression of the infiltration front during the first ten seconds after the injection. It clearly shows a progression of the infiltration by about 20 % of the raft radius in 10 seconds. The infiltration seen in Figure 1 is a combination of radial and vertical infiltration, while some test observations show the predominance of vertical infiltrations. A crust shell frozen around the raft cannot allow this behaviour. Therefore, the model should be initialized without any crust around it.

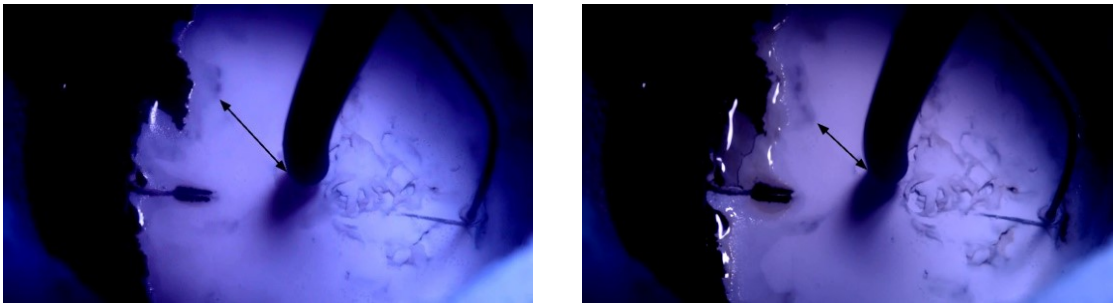

Figure 1. Displacement of the infiltration front in the first ten seconds of the raft. Left: after 2 seconds, Right: after 12 seconds.

Some adjustments have also been added to the first iteration of the model, as described later. The original version of the model did not account for the effect of gas in the pores, which strongly influenced the buoyancy of the samples. Consequently, the liquid density in the pores was adjusted, assuming that the solid-to-liquid contact was unaffected, reducing the liquid weight by 10 %. This adjustment is based on the comprehension of the bubble dynamics. Bubble formation limits dissolution and thermal transfer by lessening the solid-to-liquid contact area. However, as the bubble grows, it pushes the liquid away from the pores. This creates forced convection inside the adjacent pores, increasing the effective diffusion of dissolved alumina to the raft's surface and eventually out of the raft. Also, when the bubble escapes, fresh bath material replaces it, decreasing the alumina mass fraction in the pores, thus again promoting the heat and mass transfer between the alumina and the bath. The video recording allowed the estimation of the gas release to be at its maximum in the first two minutes and drastically lower after five minutes. A logistic function was then applied to the weight adjustment, fitting these parameters uniformly for all five scenarios.

The model accounts for various parameters and phenomena such as powder porosity, capillary infiltration, effective conductivity, heat transfer mechanisms including conduction and convection, and phase change enthalpies during the dissolution and sintering. Figure 2 show a brief overview of how the dissolution model works, while Figure 3 explain how the sintering of the alumina affects the dissolution of a raft. Numbers and letters present throughout the text and figures of the entire article refer to the predominance of the phenomenon presented in Figures 2 and 3.

First, the simulation starts with alumina powder, which is shaped into a disk with a diameter of 12 cm and a thickness proportional to the mass injected, approximately 3.6 mm for 40 g. This disk is divided into layers of 73 µm. The effective porosity (1) of the disk is then calculated, considering both intergranular and intragranular porosity. Intragranular porosity relates to the specific surface parameters of the alumina, due to its internal porosities, while intergranular porosity refers to the spaces within individual grains.

Once the effective porosity is determined, the capillary infiltration (2) of the alumina by the bath is calculated, which gives the liquid height at each time step. Next, the effective conductivity (3) of each layer of the alumina disk is computed, considering that wet layers have different thermal conductivity than dry layers. This effective conductivity allows the heat transfer calculation solely through conduction (4), considering the presence of liquid in the pores.

Then, convective heat transfer (5) is considered at the bottom of the disk, originating from the movement of the liquid. The model uses a generic heat transfer model for a flat plate with parallel flow, representing the heat flow that gradually rises through the alumina disk. The heat transfer occurring between the grains (6) and the bath is then applied to each layer of the disk, considering enthalpies for the dissolution, the phase change of the bath, and the phase change of alumina due

to sintering. At the top of the raft, radiative heat losses (7) are considered following the behavior encountered in the experimental setup, where thermal radiation to the environment occurs.

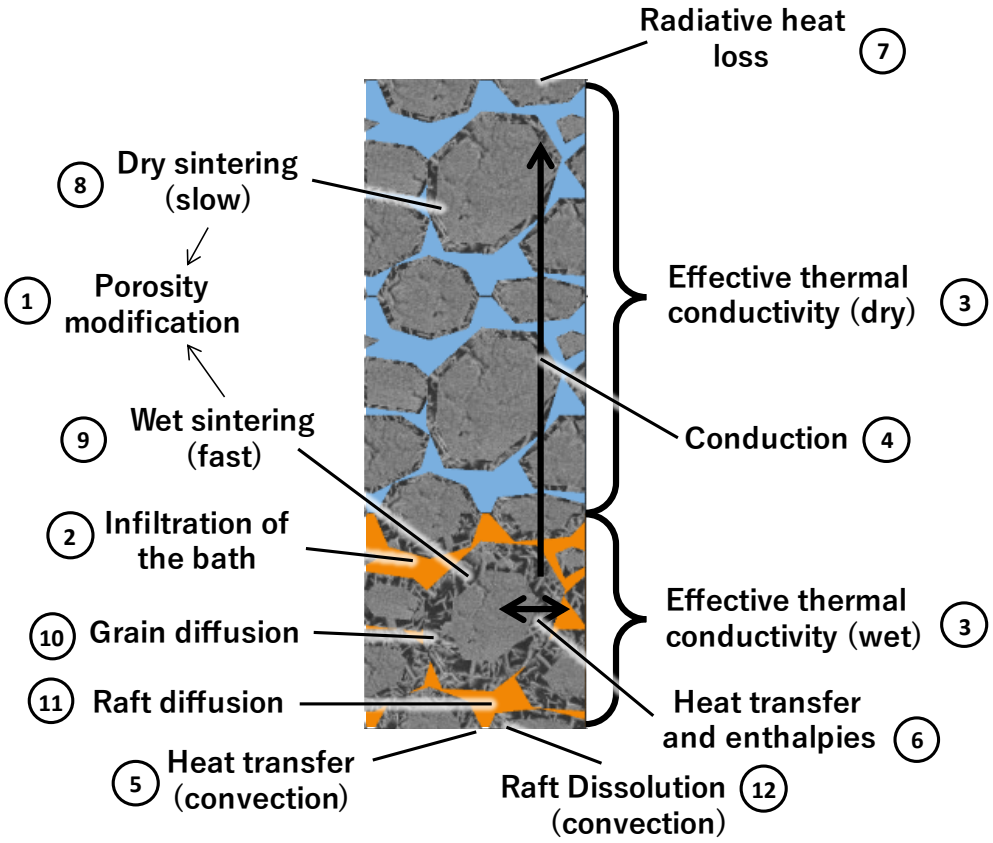

Figure 2. Overview of the model mechanisms. See the text for the description of each number.

Now, let's delve into the essential core of the dissolution of the model, **which is the sintering of alumina** (8, 9), and resumed in Figure 3**.** Through the alumina sintering, gamma alumina grains transform into alpha alumina platelets. This transformation leads to the rapid dissolution of gamma alumina grains, which then precipitate as alpha alumina (A). This precipitation occurs within the grain's intragranular porosities or on the existing alpha alumina within the grain, created during the calcination after the Bayer process. The number and size of these precipitation sites control the number and size of the resulting platelets (B). The precipitation process will transform all the dissolved alumina available in α-alumina platelets, even the one already presents in the bath, until an equilibrium state (C). This phenomenon significantly increases the intragranular porosity of the grain, and thus the area of contact between the solid and the liquid for further dissolution. Note that the grain size may increase slightly and lead to a nearly continuous matrix of alumina platelets in the raft. However, it is primarily the internal structure that changes, with the alpha alumina platelets acting as the real exchange surface between the solid and liquid phases. Once there is not enough dissolved alumina around the platelets to sustain the precipitation, the platelets will dissolve in the bath in the intergranular porosities (D).

The platelets dissolution is considered to happen by diffusion between alumina and the bath inside the intragranular porosities of the grain (10). This alumina then diffuses outward, spreading into the intergranular pores through natural convection (11). Finally, the alumina diffuses to the lower surface of the raft, where forced convection occurs, resulting in the effective dissolution of the alumina raft (12).

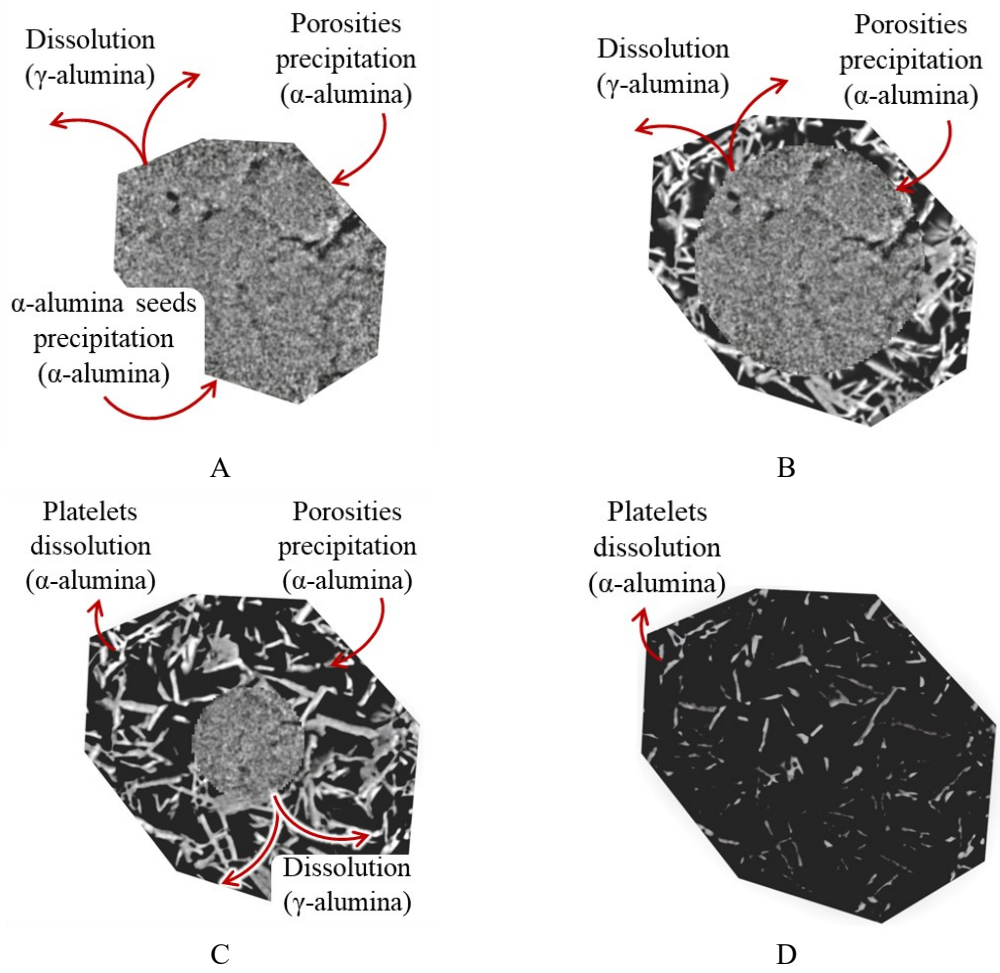

Figure 3. Sintering of the alumina grain in contact with the bath. A: dissolution-precipitation, B: platelets growth, C: platelets equilibrium, D: platelets dissolution.

It is important to note that the intragranular porosity of our raft changes during this process, altering the porosity of the entire raft layer and influencing alumina infiltration by the bath. Additionally, sintering occurs rapidly in the presence of liquid but also takes place, albeit more slowly, in the dry portion of the raft due to the presence of fluorine vapours. This modification of the intragranular porosity in the dry layers is considered in the model. From experimental observations, dry sintering takes around fifteen minutes, and wet sintering can be completed in less than two minutes.

3. Results Comparison

With these two sets of data, the comparison is now possible. For the experimental results, the mean and its uncertainty within 90 % confidence are calculated using a Student's t-distribution, due to the low number of samples for each condition. This approach provides a confidence interval around experimental results within which the dissolution model should fall, as presented in the result section.

The comparison between the model and corresponding experimental conditions is now presented. The similarities between the model and experimental results are obvious and the model explains most of the behaviour of the samples. Therefore, the five cases will be presented, regrouped in similar behaviour, and discussed. Note that the curves can be stripped down into four main phases:

the setting phase (2–6), dissolution phase (1–6, 9, 10), disintegration phase (10–12), and the thermal equilibrium plateau (7). The analysis will refer to these phases for more convenience. Each figure also presents vertical lines that indicate the phases from the model's point of view. This will help compare the different phases encountered in the model and the tests

3.1 Model Performances

The three first cases studied show the overall performance of the model to predict the dissolution of alumina near industrial conditions.

3.1.1 Case 1

The first case represents a test performed at 971 °C with low superheat and high alumina temperature, but low alumina mass fractions in the bath. The experimental results of this test are compared to the model output in Figure 4.

At first glance, significant similarities between the model and the experiments can be observed, and the four phases can be identified. The model fairly sticks in the uncertainty region around the mean of the samples (grey area). Also, the slopes of these four phases are of the same order of magnitude. The model accurately depicts a rapid increase in apparent weight due to the infiltration of the alumina raft (2), mirroring what can be observed in most of the samples tested in terms of both speed and magnitude. Then, a plateau is reached, corresponding to the well-known latent phase of the raft dissolution. Then, a rapid dissolution and disintegration phase are observed. At the end of the curve, a constant plateau is present and represents the amount of alumina that did not dissolve during the test, due to the temperature drop of the bath and the sample. This value is also well predicted by the model.

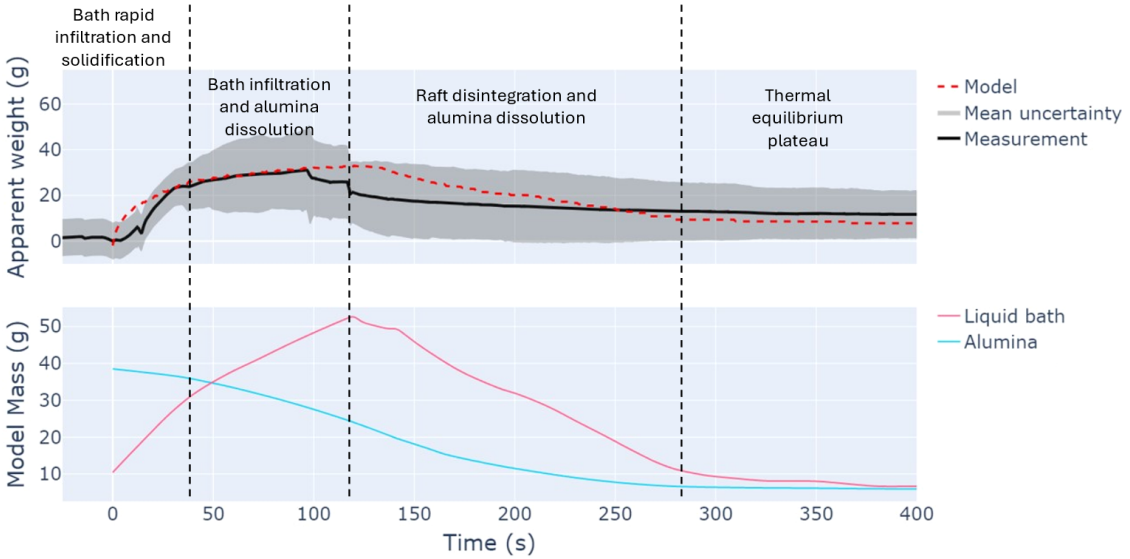

Figure 4. Comparison of the model with tests performed at 971 °C, low superheat, and bath with low alumina content. Vertical lines separate the model phases.

Setting Phase

The analysis of the output of the model for the setting phase shows that the main phenomenon is clearly the infiltration of the raft by the bath (2). The apparent weight of the raft rapidly increases with the augmentation of the bath mass inside the intergranular porosities of the raft. In the meantime, the alumina slightly begins to dissolve (10) inside the intragranular porosities of the

grains, initiating the sintering (9) of the first layers of the raft. Note also that only a small amount of solidified bath is created during this phase (6). The alumina present in the raft rapidly reaches a temperature near the liquidus of the bath due to the high heat input from the lower face of the raft.

Dissolution Phase

The dissolution phase of the raft is in fact very active. It is during that phase that the sintering of the alumina (9) is predominant. It rapidly modifies the structure of the raft, allowing more liquid to come in contact with alumina by increasing the intragranular porosities of the grains (1). Also, by doing that, it lowers the volume of the solid alumina inside the raft, allowing slightly more bath to infiltrate the raft. The alumina dissolves in the intragranular (10) and intergranular (11) porosities of the raft. The internal diffusion of the raft begins to reach its lower surface and the bulk bath (12), and despite the name of the phase, the effective dissolution of the raft is steady. However, the total mass of the raft still increases due to the infiltration of the higher layers of the raft (2).

The dissolution of the rafts mainly occurs in the body of the raft (10–11) instead of at its bottom face (12). This is due to the diffusive controlled dissolution of the grains (10) that is favoured by an increase in aluminium fluoride content. As the bath of the lower layer freezes (6), its aluminium fluoride content increases in the layer above. Therefore, an extremum can be reached so that a layer in the middle of the raft can disappear before the lower layer. This will create a horizontal, mechanically weak plane in the raft that can lead to early disintegration. This behaviour has been observed in previous work as presented by [2], where he observed snow-like disintegration and stratum shape aggregates depending on the conditions of the bath. However, the experimental setup prevents the fall of such aggregates, as for the model simulation.

Disintegration Phase

The dissolution of the raft occurs by the internal dissolution of each of the layers in contact with the liquid (10–11). Once the majority of a layer is dissolved (D), the remaining alumina and the bath that contains that layer simply vanish from the model calculations and create the disintegration visible on the graph. During that phase, the dissolution of the layers and the raft (10–12) continues until the thermal conditions prevent it.

Thermal Equilibrium

The experimental setup used to perform this work has a substantial heat loss due to the open furnace (7). Therefore, the temperature of the higher layers of the raft reaches a temperature too low to allow the dissolution. The model is able to limit the dissolution of the layers if its thermal conditions are not favourable to the dissolution and predict the remaining mass of the raft in the studied cases. This phase is inherent to the experimental setup and further discussion will focus on the three first phases only.

3.1.2 Case 2

The second case of this study concerns a test performed at 967°C with a low superheat. In this case, the alumina injected is at a low temperature in a bath with low alumina concentration and results are reported in Figure 5. The model follows the general tendencies observed in the experimental tests and the differences are easily explained by the special experimental conditions encountered.

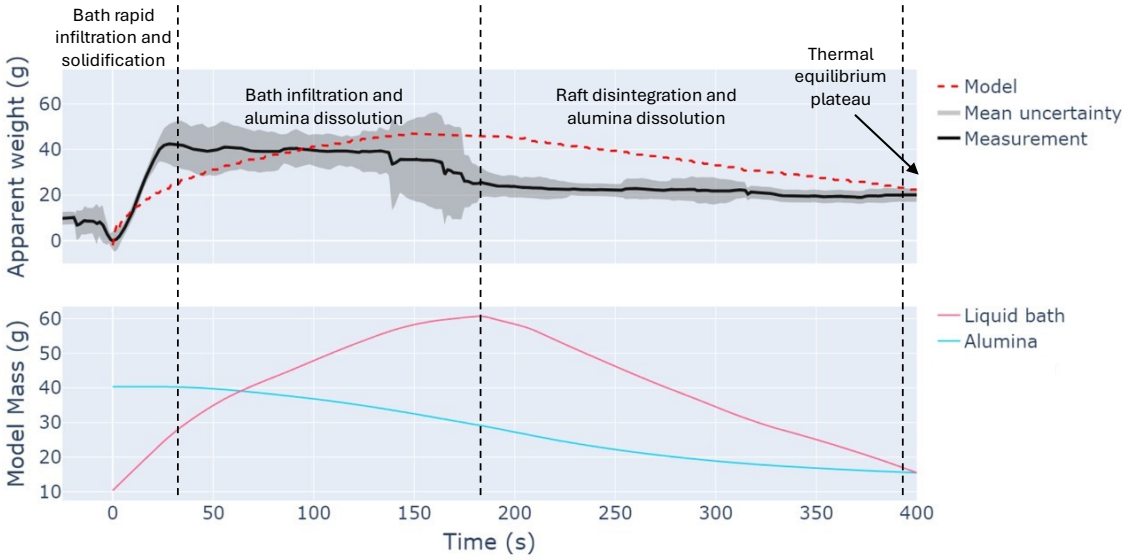

Figure 5. Comparison of the model with tests performed at 967 °C, low superheat, and bath with low alumina content. Vertical lines separate the model phases.

Setting Phase

In the tests of case two, the samples fixed themselves to the wall of the steel ring, the rapid increase of the apparent mass at the beginning of the curve is due to the bath-air interface lower than the one expected by the model. Therefore, the majority of the mass of the sample is outside of the bath and the infiltration of the powder brings that bath above the interface height, increasing the mass accordingly without augmenting the buoyancy. The general behaviour of the alumina and bath mass inside the raft is comparable to that encountered in case one.

Dissolution Phase

The samples later detach from the steel ring and provoke aggregates to suddenly sink after 140 seconds. This is the cause of the sudden drop in the apparent weight in this portion of Figure 3. Before the detachment, a significant portion of the sample was outside the bath, and thus not affected by the buoyancy. The complete immersion of the samples leads to a larger buoyancy force for the same mass and thus a lower apparent weight. In the meantime, the surface tension contribution to the apparent weight remains the same, because it affects the support of the sample that stays at the interface. These are the main reasons for the difference between the model and the experimental curves.

Note also that, between 125 s and 170 s, the uncertainty around the mean increases on both sides of the mean. In reality, the individual sample's curves only go downward at this point. That is to say that the distribution of the sample values in this area is skewed toward the lower values. However, the uncertainty calculation assumes a symmetric distribution of the samples around the mean and then applies this deviation to both sides of the mean curve. Therefore, the upward peak in the uncertainty in the 125–170 s region corresponds to the mirroring of the larger uncertainty around the mean.

Disintegration Phase

The disintegration phase, as predicted by the model is again fairly similar to that of case one. The main difference here is that the sample is completely immersed in the liquid so that the influence of the disintegration on the experimental curve is lesser due to the added buoyancy.

3.1.3 Case 3

Case three injected low alumina temperature in a bath of 981 °C with high superheat and low alumina mass fractions. Here again, the model can predict the main behaviour of the raft similarly to cases one and two.

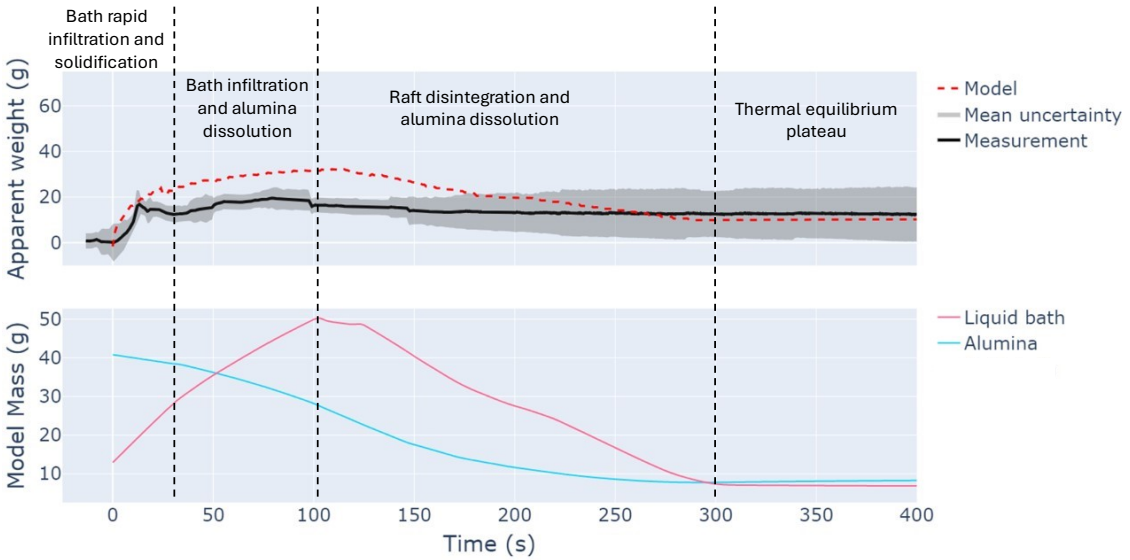

Figure 6. Comparison of the model with tests performed at 981 °C, high superheat, and bath with low alumina content. Vertical lines separate the model phases.

Setting Phase

Similar to that encountered in cases one and two, the infiltration of the liquid (2) and the dissolution of the alumina (10–11) are little impacted by the higher temperature during this phase.

Dissolution Phase

The dissolution (10) and sintering of the alumina (9) are favoured by the augmentation of the diffusivity of the alumina due to the higher temperature. This also causes the dissolution phase to end sooner than cases one and two.

Disintegration Phase

The disintegration phase is also very similar to that of cases one and two. The increase in the diffusivity that helped to hasten the end of the dissolution phase has a lesser impact on the disappearance of the layers.

3.2 Model Limitations

The two last cases studied consist of cases where the alumina content was higher than industrial conditions, along with lower temperatures. Larger differences can be there observed so that the common phase is slightly different than the first three cases and thus will not be referred to.

3.2.1 Case 4

Case four consists of an injection of cold alumina in a rich alumina bath at 932°C with a low superheat.

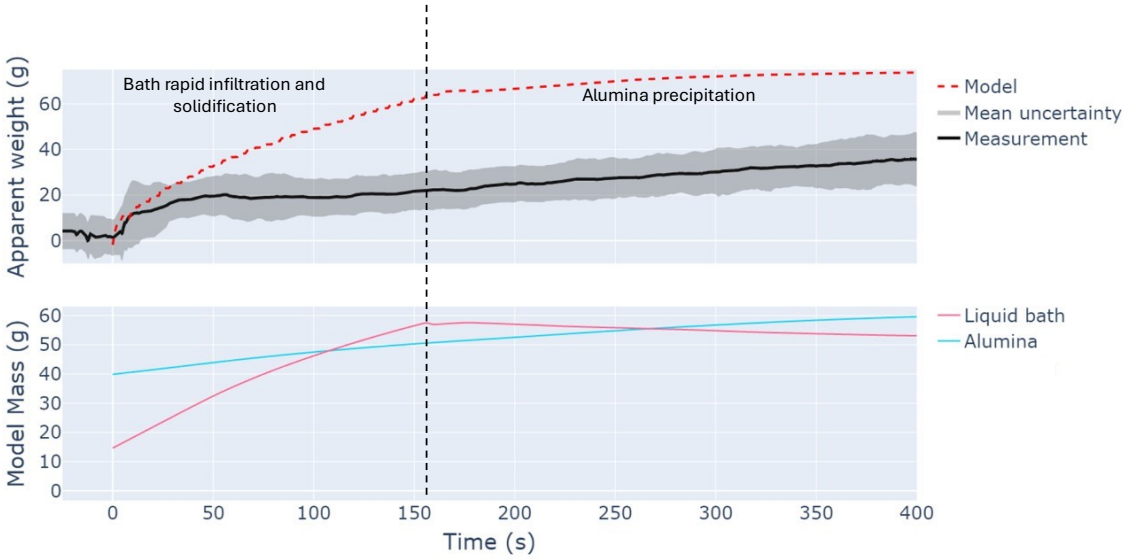

Figure 7. Comparison of the model with tests performed at 932°C, low superheat, and bath with high alumina content. Vertical lines show the model phases.

Case four is controlled by the heat available for all the phenomena involved in the dissolution process. The experimental curves, presented in Figure 7, show that infiltration occurs at the beginning of the test and that the apparent weight of the raft steadily increases from there. This creates a greater contrast between the model and the test, as indicated below.

A significant disparity stems from the model's limitation, assuming that none of its strata undergoes complete liquid-to-solid transformation. This detail is crucial because if the controlling factor of the dissolution switches from the chemical parameters to the thermal parameters, the model could diverge, as presented in case four. Such occurrences typically arise when the bath temperature is low, marked by a high additive proportion and low superheat, compounded by a low alumina injection temperature. Additionally, significant radiation losses from the raft further exacerbate this condition relative to the bath's calorific share. It's worth noting that this condition holds less sway in electrolytic cells, a topic described later. Despite these limitations, the model suggests that the alumina dissolved in the bath will precipitate on the solid alumina of the raft through the sintering process, according to the test observations.

3.2.2 Case 5

The last case tries to increase the thermal energy in a bath similar to case four. So here the alumina temperature was high, along with the superheat, added to a bath at 942 °C

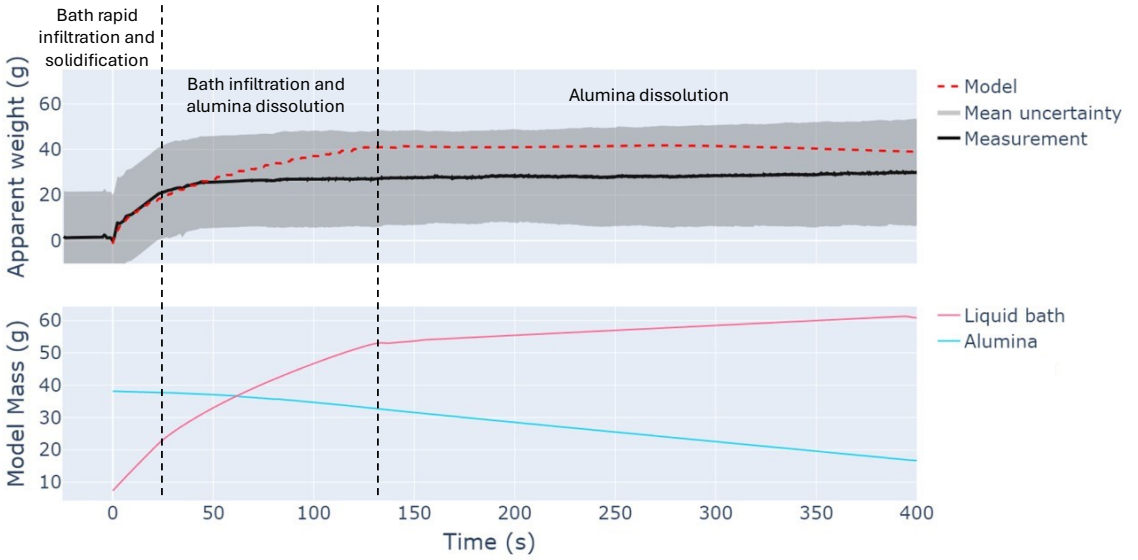

Figure 8. Comparison of the model with tests performed at 942 °C, high superheat, and bath with low alumina content. Vertical lines show the model phases.

As seen in Figure 8, the additional energy introduced in the system allowed the sample to keep a constant apparent weight throughout the whole test, as predicted by the model. Nevertheless, the details of the model clearly show that the alumina can dissolve at a constant rate. By comparison with the other case, this rate represents half of those found in cases one and three but is only 20 % lower than case two.

3.3 Improvements Avenue

Table 1 shows the differences in the time of each phase between the model and the tests. From this comparison, it appears that the performances of the model are better for the dissolution and disintegration of the rafts. Also, the model easily describes chemical-limited systems, while thermal-limited systems need more tuning. The average dissolution rate for each case is presented to help compare the general outcome of each case and represents the amount of alumina dissolved before the thermal equilibrium is achieved, from the model point of view. It can be seen that cases one and three give similar raft dissolution. Cases two and five also led to similar dissolution rate, despite their large differences in chemistry. At last, case four only achieved to precipitate alumina from the bulk bath inside the raft, due to the local lowering of the solubility.

Table 1. Comparison of the time of each phase between the model and the experimental tests.

Case	Setting			Dissolution			Disintegration			Alumina avg rate (mg/s)
	Model (s)	Tests (s)	Dev (%)	Model (s)	Tests (s)	Dev (%)	Model (s)	Tests (s)	Dev (%)	
1	35	30	16.3	85	65	30.7	165	155	6.5	- 122
2	40	25	60.0	140	110	27.3	215	180	19.4	- 63
3	30	15	50.0	70	65	7.7	150	120	25.0	- 119
4	55	10	450	100	45	220	–	–	–	+ 50
5	25	25	0	105	25	400	–	–	–	- 48

These results are inherent to several experimental limitations and from the use of some hypotheses. As described thereafter, the focus of the next development steps should aim at the description of the degassing of the alumina as it heats and sinter. The quantification of the influence of the bubble formation and release on the dissolution rate will also greatly improve the model outcome. The next section will address the limitations and the potential improvement to the model that can be implemented.

3.3.1 Experimental Tests

The exact position of the sample holder in the experimental setup itself introduces uncertainty regarding the vertical position of the experimental curves. The position of the sample holder relative to the free surface of the bath is crucial to ensure that the buoyancy force experienced by the sample is consistent. However, measurement errors in determining this interface position in this highly hostile environment are substantial compared to the dimensions of the sample. Thus, a positioning error of 1 mm in the support position, compared to the thickness of the raft, which is less than 4 mm, can cause a difference of 25 % in the contribution of buoyancy to the apparent weight of the sample. Therefore, a better positioning of the sample will greatly increase the precision of the model.

At the very beginning of the curves, a difference between the model and the experimental curve can be observed. This difference has four main causes. First, experimental injection takes up to 2 s, while the model begins when the alumina is fully injected. Second, the horizontal position of the experimental curves has been detected by the maximum value of the derivative of the different curves. Therefore, a slight difference can be estimated between the injection time and the real one for each test. Third, the mean curve represents a rolling mean on the data of half a second, which smooths the curve. At last, in the experimental curve, infiltration increases simultaneously with injection, whereas in the model, a solid block of alumina is considered already in place, resulting in a noticeable difference in infiltration timing. Anyhow, after a few seconds, these effects fade away and the model and the experimental tests show the same tendency. Note also that the size of the initial cloud of the alumina injection is not well defined and is surely influenced by the alumina's initial temperature. A better understanding of the injection dynamics will be useful to enhance the model in the first few seconds.

Regarding the right end of the curve, the vertical position of the observed plateau, both in the experimental data and the model, depends on the temperatures imposed during the dissolution. In the experimental tests, a temperature drop of nearly 20 °C between the beginning and the end of the experiment was experienced. This variation was not always linear nor the same from test to test, whereas in the model, a linear temperature loss of 20 °C from the start to the end is assumed. Again, this assumption may not precisely reflect the conditions in our experiments, as temperature changes primarily depend on radiation, resulting in a more logarithmic curve than a linear one.
The mean diameter of the alumina grains is assumed to be 80 µm in the model, while the reality can be different. This parameter will influence the capillarity inside the raft and thus change the infiltration speed.

3.3.2 Bubbles

During the dissolution phase, the samples experience degassing from the heating of the gases adsorbed on the surface of the alumina grains and trapped inside their volume. The model does not account for that phenomenon of great importance for the raft dissolution. The formation of bubbles in the pores between the grains will displace the liquid from these areas as the bubbles grow. Bubbles in the intergranular pores will then limit the heat and mass transfer in this zone.

However, they also push the liquid upwards or downwards, accelerating the infiltration of the upper layers and artificially increasing the transport of alumina towards the bath. Conversely, when the bubble escapes, the fresh bath will replace the gas, promoting local alumina dissolution as well as heat transfer between the cryolite and the interior of the raft. Additionally, degassing promotes mechanical damage to the weakest part of the raft, which further facilitates its disintegration in this portion of the curve. The degassing kinetics is also suspected to depend on the temperature of the system. The desorption of adsorbed gases on the surface and crystalline water contained within the alumina is enhanced by temperature. Modelling the vaporization behaviour of this water is necessary for improved model fidelity. For the moment, the model only considers a diffusive dissolution of the alumina on a raft. Therefore, the dynamic of the bubble effect on the overall dissolution rate is not yet taken into account but is assumed to be similar to that of a continuous diffusive dissolution. Future steps will address and integrate the handling of this issue directly into the dissolution model.

3.3.3 Heat and Mass Transfer

At this point, the solidification of the bath in the calculations does not alter the raft porosity, neither intragranular nor intergranular, and the availability of the liquid for further infiltration. Therefore, the infiltration is overestimated in the cases where the bath solidification is non-negligible. Nevertheless, the slope of the infiltration step is lower than in the other cases.

Another disparity between experimental results and the model lies in the contact surface between the liquid and solid phases. While the model assumes a perfect 12 cm diameter alumina disc dissolving with a current parallel to its surface, our experimental setup slightly differs. In reality, the flow is not exactly parallel to the sample, as it descends towards the centre of the crucible as it progresses. Additionally, the exchange surface area between the raft and the liquid in our experimental setup decreases over time for the samples with high dissolution rates. This reduction occurs due to the formation and growth of platelets within the alumina disc, a phenomenon observed in our dissolution videos. These platelets alter the exchange surface, leading to fluctuations in dissolving behaviour. Moreover, episodes of disintegration further influence the process, a factor not yet incorporated into the one-dimensional model due to its lack of mechanical resistance characteristics. Consequently, these factors contribute to the differences observed between experimental and modelled dissolving plateaus.

The modelling of the dissolution and disintegration phases can benefit from a better understanding of the role of the specific surface of the alumina and its alpha phase content. These two parameters assumed constant in the model, drive the number of platelets created during the sintering process by acting as precipitation sites for the dissolved alumina. Therefore, using the right characterization of these parameters will greatly influence the effective dissolution surface of the alumina, and thus the dissolution rate predicted by the model.

4. Industrial Applications

As mentioned earlier, the conditions within electrolytic cells differ from those simulated in the laboratory and by the model. In our experimental setup, alumina injections were performed at 25 °C, whereas in industry, storing alumina above the cell typically results in injection temperatures rarely dipping below 100 °C. This temperature disparity entails a significant energy difference from injection made at 25° C, allowing more conditions to be controlled by the bath chemistry instead of thermal energy. Moreover, radiation losses experienced by the raft and the bath would vary significantly, with the crust above the anodes and the bath creating substantial thermal isolation from the environment. Consequently, radiation losses would be considerably diminished. To precisely gauge this effect, the temperature of the crust at its lower face should be

considered, likely higher than 700 °C as presented by [3] . At this juncture, dissolution would be significantly facilitated. However, conditions at the injection hole could vary, depending on whether it is open or closed. A closed hole will help to heat the alumina contrary to an open one. Regardless, a closed hole will also completely change the injection behaviour of alumina, which can therefore be very different from the analysis presented here.

In the experimental setup, a 20 °C loss was observed from the start to the end of the experiment, which substantially altered alumina dissolution and was also imposed on the model. However, such conditions do not reflect the cell operations, where temperatures remain relatively stable. It is also well known that the bath temperature at the centre of the cell can differ by several degrees Celsius from that measured at the tapping hole. Therefore, the superheat could exceed predictions at the dissolution site, thus promoting dissolution. Under these thermal conditions, it is unlikely that thermal factors limit the dissolution process in industrial cells.

To obtain a more realistic picture, an attempt to ascertain the influence of operational parameters on alumina dissolution is now presented using the same model presented above. These tests assume a standard bath composition of 11.5 % of AlF_3, 5.5 % CaF_2, and 3 % of alumina. Also, the superheat of the bath is 10 °C, the alumina injection temperature is 150 °C and the environment temperature is 300 °C, which is still very conservative. From this base bath composition, each parameter is varied one by one to obtain the main effect for each parameter, as presented in the Figure 9. The model considers that the liquid flow pattern and velocity are constant over all the scenarios. Therefore, the Reynolds number that drives the heat and mass transfer underneath the raft is affected according to the bath's chemical composition, through the viscosity and density variation. The vertical axis is normalized around the mean of the remaining alumina mass after 200 s. This means that a negative value will lead to a lower alumina mass of the raft after 200 s and that the dissolution is promoted.

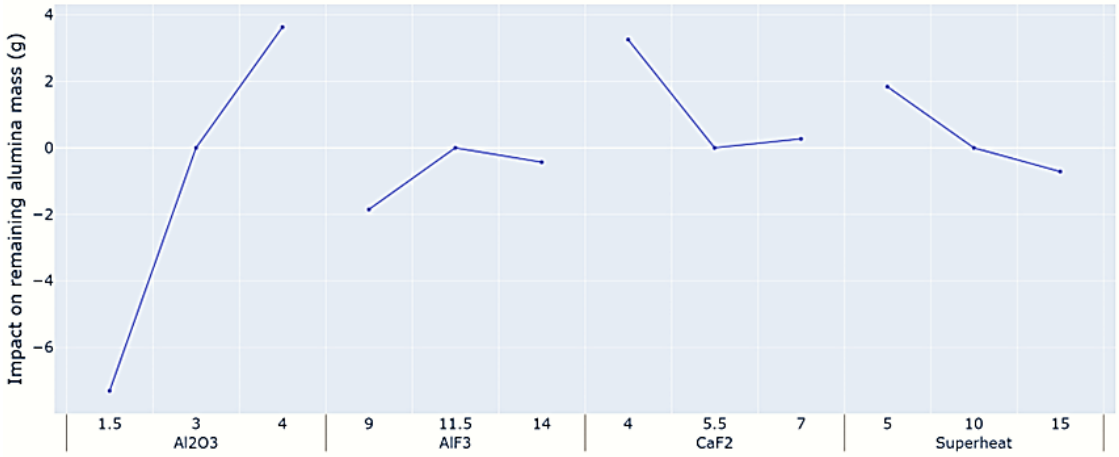

Figure 9. Main effect of the parameters of the model on the remaining alumina mass after 200 seconds.

The main effect figure shows that the increase of the additives in the bath composition does not limit the dissolution of a raft, except for the alumina mass fraction, which is a strong limiting factor. A slight increase in the dissolution of the raft can also be observed in the case of aluminium fluoride, compared to the reference case. This augmentation in the dissolution can be explained by the increase in the diffusivity of the dissolved alumina in the body of the raft. A look at the results of the model (Figure 2 to 6) shows that the dissolution of the alumina increases as the liquid rises in the raft. As explained above, the dissolution of the raft is controlled by the internal diffusivity of the dissolved alumina. Therefore, the lower solubility limit of the bath is

counterbalanced by the augmentation of the diffusivity. However, be aware that this is only true when the raft has a significant thickness, in which the diffusion is significant. This is an important statement that explains the difference between the results of this work with the results of other works, where the thickness of the raft was usually negligible. If the raft is very thin, the dissolution of the raft is controlled by convective mass transfer, itself driven by the alumina solubility. However, a taller raft will bring more dissolved alumina to the lower face of the raft by the diffusion in its pores.

These results state that the limiting factor for the alumina dissolution is the diffusivity of the dissolved alumina in the cryolite melt. Therefore, increasing the mass fraction of additives in the bath can promote dissolution. Nevertheless, be aware that this conclusion is strongly dependent on the calculation of the alumina diffusivity from the Wilke-Chang equation, as presented in [4].

5. Conclusions

A model for the alumina dissolution using thermal and chemical conditions has been developed in this work. This model simulates the main reactions of the dissolution of an alumina raft:

- Bath infiltration and solidification
- Alumina sintering and dissolution
- Heat transfer and enthalpy changes

This model was compared to five experimental conditions of alumina powder injection. The model can predict the actual weight of the raft created in the conditions near industrial cells. The model was then used to find the main effects of the thermal and chemical conditions on the raft dissolution. This sheds light on the raft dissolution that is limited by its internal diffusion. Therefore, increasing the diffusivity of the dissolved alumina within the raft body will enhance the overall dissolution rate of the raft. An augmentation of the additive content is then favourable to the dissolution of the raft with a significative thickness. In the case of a thin raft, the diffusivity has a lesser impact on the dissolution rate as it is controlled by fluid convection.

The next step to improve the prediction capabilities of the model is to understand the bubble dynamics inside the raft and its influence on the dissolution rate of alumina.

6. References

1. Jonathan Alarie et al., Dimensional Analysis Applied to the Dissolution and Disintegration of Alumina Rafts: The Riddle of Dissolving Alumina Rafts Solved, *Light Metals* 2024, 621-629.
2. Jonathan Alarie et al., Determination of the Alumina Diffusivity and Dissolution Rate for Alumina Samples Immersed in a Cryolitic Bath, *Materialia*, Volume 32, December 2023, 101901.
3. László Istvan Kiss, Alumina Dissolution - a Critical Step in Aluminum Electrolysis, *Keynote session presented at the TMS* 2018, 11-15 March 2018, Phoenix, Arizona, U.S.A.
4. A. Kovács et al., A Heat and Mass Transfer Problem for the Dissolution of an Alumina Particle in a Cryolite Bath, *International Journal of Heat and Mass Transfer*, 2020, Volume 162, 120232.